Phase-Compensated Conformal Antennas for Changing Spherical Surfaces

Benjamin D. Braaten, *Member, IEEE*, Sayan Roy, *Student Member, IEEE*, Irfan Irfanullah, *Member, IEEE*, Sanjay Nariyal, *Member, IEEE*, and Dimitris E. Anagnostou, *Senior Member, IEEE*

***Abstract*—Self-adapting conformal antennas for changing spherical surfaces are investigated in this work. More specifically, the theory on the relationship between the radius of the spherical surface, element spacing of the conformal array and required phase compensation is developed. Initially, for theoretical validation, a 4 × 4 phased array antenna is assembled with individual microstrip antennas used as the radiators at 2.47 GHz. Each antenna is connected to a commercially available voltage controlled phase shifter with identical SMA cables and then each phase shifter is connected to a port on a sixteen-way power divider. This phased-array antenna allows for convenient placement of individual patches on the spherical surface and precise phase control. For further validation, a second 4 × 4 phased-array antenna with embedded phase shifters and a sensing circuit is manufactured. The sensing circuit is used to measure the radius of curvature of the spherical surface and use this information to autonomously apply the appropriate phase compensation, based on the previous theoretical developments, to recover the radiation pattern of the array for different spherical surfaces at 2.47 GHz. Overall, good agreement between theory, simulation and experimental data is shown and that it is possible to recover the radiation pattern autonomously.**

***Index Terms*—Conformal antennas, microstrip arrays, phased arrays, spherical arrays.**

I. Introduction

CONFORMAL antennas are used in many applications where unique antenna placement is required. This may include the integration of an antenna on a vehicle or aircraft [1]–[5], circular arrays for wider coverage than planar antennas [6]–[8], textile antennas for systems being integrated into a wearable wireless network [9]–[12] or unique composites for embedding the antenna into a structure for load-bearing purposes [13]. For many of these applications, antenna systems are required to operate with greater radiation efficiency, more adaptive beam-forming capabilities, cost effective RF electronics and structural robustness and furthermore, these requirements are to be met in complex radiation environments that include multiple radiators and changing or vibrating surfaces. Because of the complex nature of these applications, many new research areas on E-textile conductors [14], metalized fibers [15] and embroidered RF circuits [16] have been developed. The results from these efforts have been very useful and have addressed many of the problems associated with physically implementing conformal antennas; however, the radiation properties of these conformal antennas can be severely degraded due to unwanted surface deformations [17]–[19].

Previous work has shown that with appropriate active and passive mechanical dampening [5], actuators [20], mechanical steering [21], [22] and voltage amplitude and phase compensation [17], [23]–[31] the radiation pattern can be improved as the shape of a conformal antenna changes. More specifically, the work in [5] mentions the use of reinforcement and active shape control at various global and local levels for compensation while the actuators in [20] are used to change the orientation of parasitic elements of an array to compensate for different radiation environments. However, with the exception of the array in [17], these compensation techniques can be quite complicated because micro-servos, sophisticated control techniques, extensive signal processing and unique RF circuitry are required.

The objective of this work is to develop a cost-effective self-adapting conformal antenna array that can autonomously preserve the radiation pattern as the spherical surface that the antenna is attached too changes radius (r). An illustration of the problem being considered is shown in Fig. 1. The self-adapting antenna array being developed here includes a unique theoretical approach that will describe the phase behavior of antenna arrays on spherical surfaces in terms of the spherical shape and element spacing. It will be shown that by deriving a relationship between the radius of the spherical surface, element spacing and the phase behavior of the radiated wave, a compact inexpensive sensor circuit can be designed and implemented (using this relationship) into the layout of a conformal antenna to autonomously preserve the radiation pattern. Furthermore, this work is different from [17] because the theory developed in [17] is restricted to 1-D surfaces (i.e., singly curved surfaces). The research here is in a much more general setting that includes 2-D conformal surfaces (i.e., double curved surfaces). Moreover, the theory developed here can be used in many more applications than the theory in [17]. Some of these applications include 1) the vibrating fuselage of an aircraft, 2) protective clothing that moves on search and rescue personnel, 3) surfaces in environments that may deform due to drastic temperature changes (i.e., spacecraft) and 4) moving surfaces on vehicles.

Manuscript received June 22, 2013; revised October 15, 2013; accepted December 08, 2013. Date of publication January 09, 2014; date of current version April 03, 2014. This work was supported in part by NASA ND EPSCoR under agreement number NNX07AK91A and in part by the Department of Defense DARPA MTO Young Faculty Award number N66001-11-1-4145.

B. D. Braaten, S. Roy, I. Irfanullah, and S. Nariyal are with the Department of Electrical and Computer Engineering, North Dakota State University, Fargo, ND 58102 USA (e-mail: benbraaten@ieee.org).

D. E. Anagnostou is with the Department of Electrical and Computer Engineering, South Dakota School of Mines and Technology, Rapid City, SD 57701 USA.

Color versions of one or more of the figures in this paper are available online at http://ieeexplore.ieee.org.

Digital Object Identifier 10.1109/TAP.2014.2298881

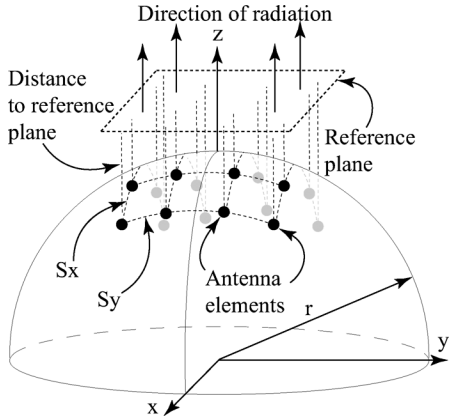

Fig. 1. Illustration of the self-adapting array on a sphere with radius r.

II. Self-Adapting Antenna Arrays on Doubly Curved Surfaces

In this paper, the theoretical derivations will be for a general $N \times N$ array on a spherical surface; however, for illustration the 4×4 array defined in Fig. 1 will be considered. Furthermore, it will be assumed that the desired radiation is in the z-direction, that the spherical surface is nonconducting (i.e., styrofoam) and that the corrected radiation pattern is defined to be the pattern with lobes and nulls comparable to the analytical computations. Similar derivations can be carried out for arrays with an odd number of elements on a side (i.e., a 5×5 array).

A. Phase Compensation Derivations

Each element of the array on the spherical surface in Fig. 1 is shown as a black dot with an element spacing of S_x and S_y in the x- and y-directions, respectively. One method for establishing radiation in the z-direction is to ensure that each field component from the antenna elements on the sphere arrive at the reference plane with the same phase, where the reference plane is parallel to the x-y plane. This will essentially create a broad-side radiation pattern to the reference plane.

To introduce the required phase for radiation in the z-direction, voltage controlled phase shifters can be used to individually adjust the voltage phase feeding each antenna element. More specifically, the amount of phase to be introduced by the phase shifters is equal and negative to the amount of phase introduced by the propagation of each field from the antenna elements on the sphere to the reference plane. In other words, a positive phase will be introduced by the voltage controlled phase shifters to cancel the negative phase that is introduced by the wave propagating toward the reference plane. This will then result in field components from each antenna element arriving at the reference plane with the same phase or zero relative phase shift between elements at the reference plane. Therefore, to compute the amount of phase introduced by the propagation from individual elements toward the reference plane, the distance from the antenna elements to the reference plane must be determined.

This distance can be determined by first considering the top view of the array on the spherical surface in Fig. 2. The view shows the antenna elements on the sphere denoted as a_{11} through a_{44} placed in equi-phase rings which are illustrated

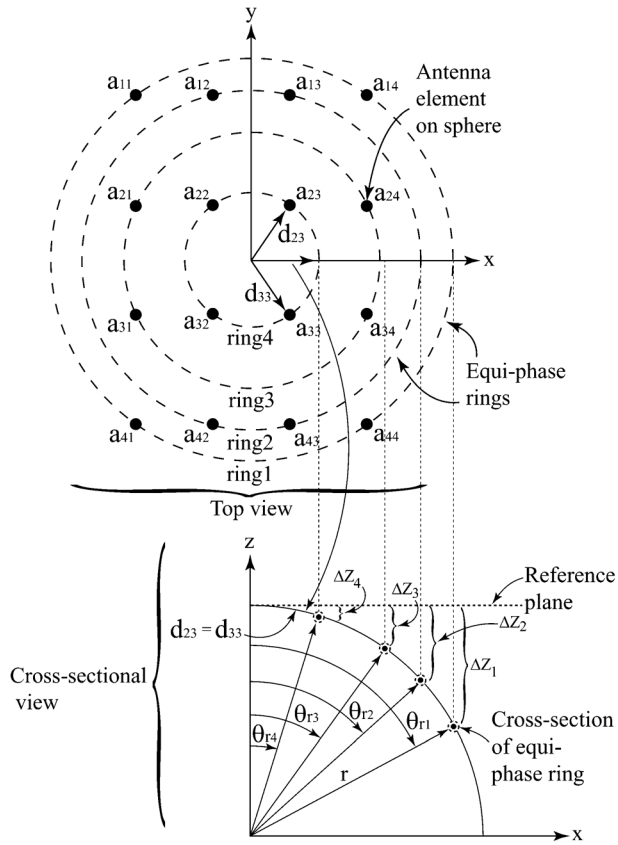

Fig. 2. (Top) View of Fig. 1 from the z-axis, showing the antenna elements on the sphere and the equi-phase rings (the sphere is underneath the reference plane) and (cross-sectional view) phase shift due to surface curvature for the adaptive array.

as dotted rings. The equi-phase rings are used to group the elements in the array that require the same amount of phase compensation. The rings can also be thought of as the elements that are at the same latitude on the spherical surface. The distance from the origin to each element along the surface of the sphere can be written in terms of the element spacing in the following manner:

$$d_{m,n} = \sqrt{(mS_y + S_y/2)^2 + (nS_x + S_x/2)^2} \qquad (1)$$

where $m = 0, 1, 2, \ldots, N/2 - 1$ is the row and n is the column location of each antenna element with $0 \leq n \leq m$. This distance can also be understood by imagining the array on a flat surface with element spacing S_x and S_y. Equation (1) can then be used to compute the distance along the flat substrate from the origin to each antenna element. Then, by placing this flat antenna array on the surface of the sphere, the inter-element spacing along the substrate is still the same and can be computed using (1). Except when the array is on the sphere, the distance is an arc length. Therefore, the following expression can be used to determine the angle $\theta_{m,n}$ (measured from the +z-axis) that describes the location of each element on the sphere:

$$\theta_{m,n} = \frac{1}{r}\sqrt{(mS_y + S_y/2)^2 + (nS_x + S_x/2)^2}. \qquad (2)$$

Next, the reference plane is defined to be at the top of the upper-hemisphere with radius r in Fig. 1. The reference plane in

Fig. 1 is drawn above the upper-hemisphere for illustration purposes only. A cross section of this definition is shown in Fig. 2. The point at which the equi-phase ring intersects the x-z plane is denoted as a black dot surrounded by a dashed ring. Since the antenna elements in the same equi-phase ring are the same distance from the reference plane (i.e., at the same latitude), a cross section of the problem can be considered for simplicity and the distance of the x-z intersection of each ring to the projection plane can be computed. Furthermore, since the equi-phase rings are centered about the origin, the distance from the z-axis to the x-z intersection of the rings along the sphere (i.e., arc length) can be computed using (1). Once this length is known, the angles θ_{rp} in Fig. 2, where $p = 1, 2, 3$ or 4, can be computed using (2). It should be noted that because of symmetry, several combinations of m and n will give the same value of θ_{rp}. When considering the computation of θ_{r4} in Fig. 2, $(m, n) = (2, 3)$ and $(m, n) = (3, 3)$ will give the same values (as illustrated with $d_{23} = d_{33}$ in Fig. 2).

Next, the distance Δz_p in Fig. 2 can be computed as

$$\Delta z_p = r(1 - \sin\theta_{rp}) \tag{3}$$

where $p = 1, 2, 3$ or 4. Then, the phase introduced by the propagation of the field from the antenna element in each equi-phase ring to the reference plane can be computed as

$$\Delta\phi_p = -jk\Delta z_p. \tag{4}$$

Therefore, the appropriate phase compensation (i.e., the phase to be introduced by the voltage controlled phase shifters) for each ring to ensure that each field arrives at the reference plane with the same phase can be computed as

$$\Delta\phi_{c,p} = -\Delta\phi_p. \tag{5}$$

Equation (5) is a relationship between the element spacing of the array on the sphere, the radius of the sphere and the number of elements on the sphere. Equation (5) will be used next to design a sensing circuit for determining the radius of curvature of the sphere and apply the appropriate phase compensation to recover the radiation pattern of the array autonomously.

B. The Sensing Circuit

For demonstration and measurement validation purposes, two 4 × 4 microstrip phased-array antenna prototypes were designed for placement on various spherical surfaces (i.e., placement on doubly curved surfaces). The sensing circuit will be embedded into the design of one of the 4 × 4 phased-array antenna prototypes. The center frequency will be 2.47 GHz and the element spacings will be $S_x = 0.45\lambda$ and $S_y = 0.6\lambda$. For these spacings, the normalized phase compensation between the four equi-phase rings versus radius of curvature r was computed using (5) and is shown in Fig. 3(a). Ring 4 was used as a reference phase to compute $\Delta\phi_{norm}$. The phase shifters used for this work were manufactured by Hittite Microwave Corporation [32] (part number: HMC928LP5E). To compute the required voltage to control the phase shifter as r changes, a linear approximation of the phase-shift versus control voltage $V_{\rm ctrl}$ was used. In particular, for $2.8 \le V_{\rm ctrl} \le 10.0$ V the following linear approximation was used to analytically compute

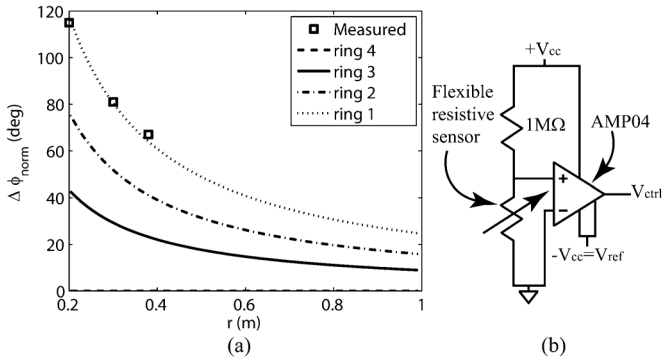

Fig. 3. (a) Required inter-element ring phase shift for different spherical radius values and (b) a schematic of the sensor circuit ($+V_{cc} = 10.0, -V_{cc} = V_{\rm ref} = -1.7$ V and $R_{\rm gain} = 1.04$ kΩ).

the normalized phase shift from the Hittite phase shifter (in degrees):

$$\Delta\phi_{\rm shift} = 33V_{\rm ctrl} + 80. \tag{6}$$

Equation (6) was determined experimentally with a series of measurements and the accuracy was checked by comparing the computed values to the data sheet of the phase shifter. $\Delta\phi_{\rm shift}$ can then be computed by using (5) and the required control voltage from the sensing circuit can be computed from (6). This then resulted in the equivalent circuit shown in Fig. 3(b) where the gain resistor was connected between pins 1 and 8. Finally, the sensing circuit was fabricated and connected to a connectorized Hittite phase shifter for evaluation. The flexible resistive sensor, manufactured by Spectra Symbol [33], was then attached to three commercially available nonconducting spheres with $r = 20.32$ cm, 30.48 cm and 38.1 cm and the phase shift introduced by the Hittite phase shifter was then measured with a network analyzer. The results from these measurements are shown to agree with the analytical computations in Fig. 3(a). The phase shift for ring 1 is only shown. To introduce the required control voltages for rings 1–4, ring 1 was connected to the sensor circuit, ring 4 was connected to 2.8 V and three resistors were connected (to provide voltage division) between rings 1 and 2, 2 and 3, and 3 and 4. This then provided the required voltages at each ring simultaneously throughout the antenna design to apply the appropriate phase compensation.

III. The 4 × 4 Conformal Antenna Array Test Platform Design

A. Configuration

To validate the theoretical developments in the previous section, the antenna test platform in Fig. 4(a) was constructed. The elements of the array consisted of individual microstrip patches designed to operate at 2.47 GHz with a spacing of 0.8λ. Each patch was printed on a single grounded Rogers 5880 RT/duroid substrate ($\varepsilon_r = 2.2$, $\tan\delta = 0.0009$) [34] with a thickness of 1.575 mm. Then each element was connected to a commercially available connectorized voltage controlled phase shifter manufactured by Hittite Microwave corporation [this is the same phase shifter used for the measurements in Fig. 3(a)] with identical SMA cables (i.e., same length and electrical properties).

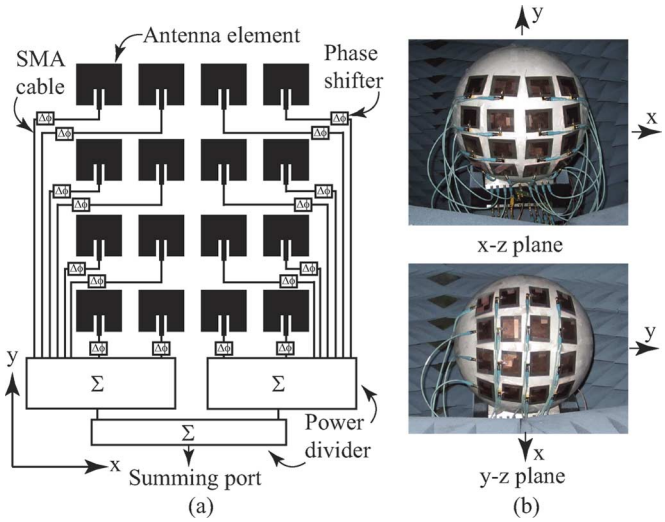

Fig. 4. (a) Diagram of the 4 × 4 phased-array antenna test platform and (b) picture of the antenna test platform being measured in the anechoic chamber on a spherical surface with a radius of $r = 20.32$ cm.

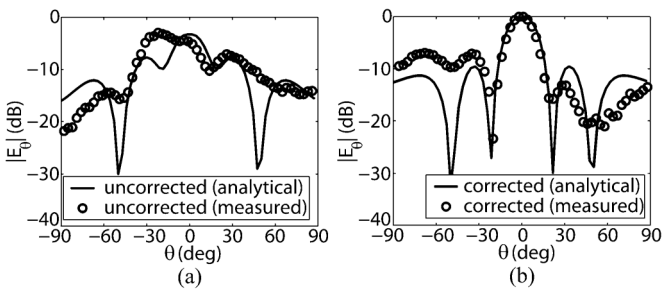

Fig. 5. (a) Analytical and measured (a) uncorrected and (b) corrected patterns at 2.47 GHz in the y-z plane for the antenna test platform on a spherical surface with a radius of $r = 20.32$ cm.

Each phase shifter was then connected to a 16 way power divider. The normalized phase compensation values (with ring 4 as the reference) were then computed using (5) and determined to be $\Delta\phi_{r1} = 284.1°$, $\Delta\phi_{r2} = 164.1°$ and $\Delta\phi_{r3} = 34.1°$. This meant that all the elements in equi-phase ring 1 were fed with a phase of 284.1°, all the elements in ring 2 were fed with a phase of 164.1° and the elements in ring 3 were fed with a phase of 34.1°. This test platform was developed to validate the expression in (5) without the affects of the sensor circuit or microstrip feed network.

B. Pattern Correction Results

A picture of the test platform being measured (in a calibrated anechoic chamber) in the x-z and y-z planes on a nonconducting styrofoam sphere is shown in Fig. 4(b) for $r = 20.32$ cm. The y-z plane results from these measurements are shown in Fig. 5(a) and (b). The x-z plane results were similar and obtained in the same manner as the y-z plane results by rotating the sphere with the test platform attached.

Next, the following expressions for the radiation pattern of a spherical array reported in [7] were used to compute the analytical results in Fig. 5(a) and (b):

$$\bar{E}(\theta,\phi) = \sum_{n=1}^{N} w_n e^{jk[x_n(u-u_s)+y_n(v-v_s)+z_n\cos\theta]} e^{j\Delta\phi_{c,p}} \quad (7)$$

where $\Delta\phi_{c,p}$ is the phase compensation term of the pth equi-phase ring with element $a_{m,n}$ and computed using (5). Equation (7) assumes a spherical coordinate system where $u = \sin\theta\cos\phi$, $u_s = \sin\theta_s\cos\phi_s$, $v = \sin\theta\sin\phi$, $v_s = \sin\theta_s\sin\phi_s$, θ_s is the elevation steering angle, ϕ_s is the azimuth steering angle and w_n is the complex weighting function. Each complex weighting function was defined as $w_n = e(\theta,\phi)$ where the expressions reported in [35] for a rectangular microstrip antenna were used as element patterns $e(\theta,\phi)$. The uncorrected results in Fig. 5(a) are the radiation patterns in the y-z plane with the voltage on each phase shifter set to the same value. This means that the field radiated from each element has a similar phase and no phase compensation has been implemented. The results in Fig. 5(b) are applying the appropriate phase compensation to rings 1–3. Overall, reasonable agreement between the analytical and measured uncorrected and corrected radiation pattern can be observed in Fig. 5(a) and (b). This indicates that the computations using (5) are correct and that the radiation pattern of a conformal antenna can be corrected with a simple analytical expression. It should also be mentioned that similar agreement between the measured and analytically computed uncorrected and corrected patterns was observed in the x-z plane.

IV. The 4 × 4 Self-Adapting Array Design

A. Layout of the Autonomous Adaptive Array

A 4 × 4 phased-array microstrip antenna prototype with interelement spacings of $S_x = 0.45\lambda$ and $S_y = 0.6\lambda$ was designed next. The array topology is shown in Fig. 6(a). The flexible substrate chosen was a Rogers 6002 RT/duroid substrate ($\varepsilon_r = 2.94$, $\tan\delta = 0.0012$) with a thickness of 0.508 mm [34]. This antenna array included the same Hittite voltage controlled phase shifters and sensing circuit reported in Section II embedded into the design. By keeping the spacing similar to the spacing used in the computations in Fig. 3(a), the sensing circuit in Fig. 3(b) could be directly embedded into the prototype design.

B. Measurement Results

1) Spherical Surface With $r = 20.32$ cm: The prototype antenna was first placed on a styrofoam spherical surface with a radius value of $r = 20.32$ cm and the corrected and uncorrected S-parameters and radiation patterns were measured (in a calibrated anechoic chamber) in both the x-z and y-z planes. The unnormalized phase compensation values were again computed using (5) and determined to be $\Delta\phi_{r1} = 131.1°$, $\Delta\phi_{r2} = 90.2°$, $\Delta\phi_{r3} = 57.7°$ and $\Delta\phi_{r4} = 15.0°$. This means that elements a_{11}, a_{14}, a_{41} and a_{44} had a phase compensation of $\Delta\phi_{r1}$, a_{12}, a_{13}, a_{42} and a_{43} had a phase compensation of $\Delta\phi_{r2}$, a_{21}, a_{24}, a_{31} and a_{34} had a phase compensation of $\Delta\phi_{r3}$ and a_{22}, a_{23}, a_{32} and a_{33} had a phase compensation of $\Delta\phi_{r4}$. A picture of the prototype antenna attached to a spherical surface with $r = 20.32$ cm is shown in Fig. 6(b). The results from these measurements in the y-z plane are shown in Figs. 7 and 8. Patterns with similar geometry (due to symmetry) were also observed in the x-z plane. The gain improvement G_Δ, which is the difference

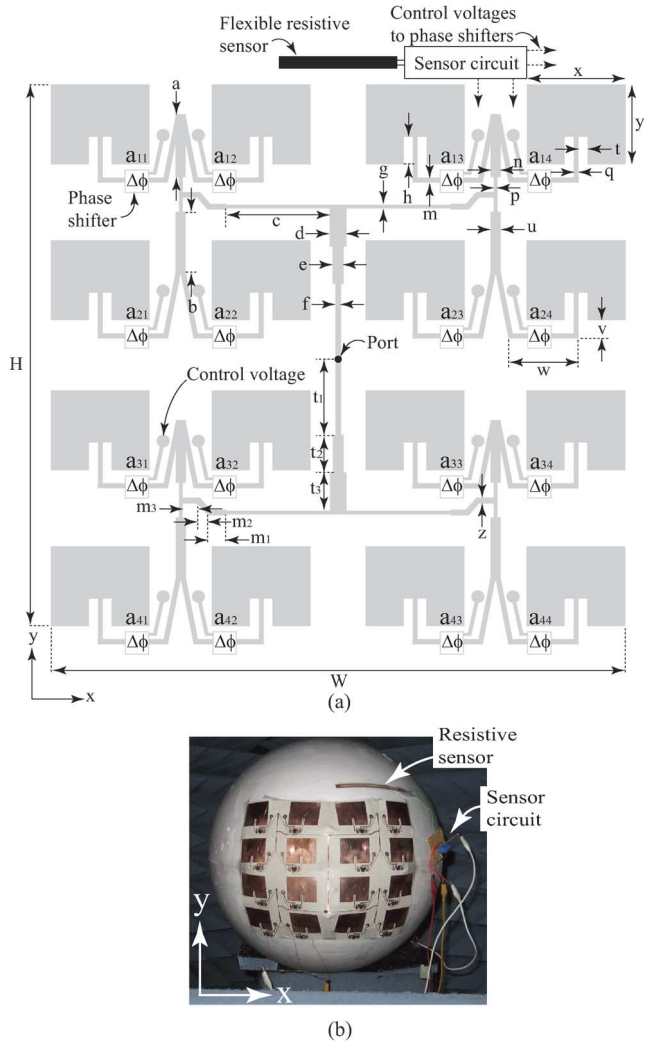

Fig. 6. (a) Drawing of the 4 × 4 prototype antenna and (b) an image of the array prototype being measured in the anechoic chamber on a spherical surface with a radius of $r = 20.32$ cm ($a = 18.18$ mm, $b = 18.18$ mm, $c = 57.0$ mm, $d = 2.8$ mm, $e = 2.4$ mm, $f = 1.0$ mm, $g = 0.8$ mm, $h = 10.0$ mm, $m = 0.8$ mm, $m_1 = 4.0$ mm, $m_2 = 6.8$ mm, $m_3 = 5.2$ mm, $n = 1.9$ mm, $p = 0.8$ mm, $q = 1.0$ mm, $t = 1.0$ mm, $t_1 = 18.7$ mm, $t_2 = 26.9$ mm, $t_3 = 7.5$ mm, $u = 1.9$ mm, $v = 8.9$ mm, $w = 21.8$ mm, $x = 43.2$ mm, $y = 35.1$ mm, $z = 1.9$ mm, $W = 268.8$ mm and $H = 195.7$ mm).

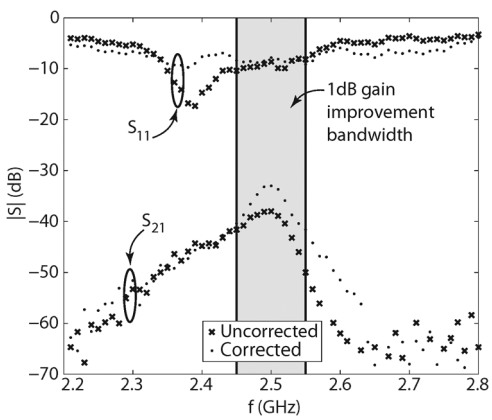

Fig. 7. Measured S-parameters for the prototype on a spherical surface with a radius of $r = 20.32$ cm.

between the corrected and uncorrected cases, at 2.47 GHz are shown in Table I. A 2.6 dBi improvement in gain was observed.

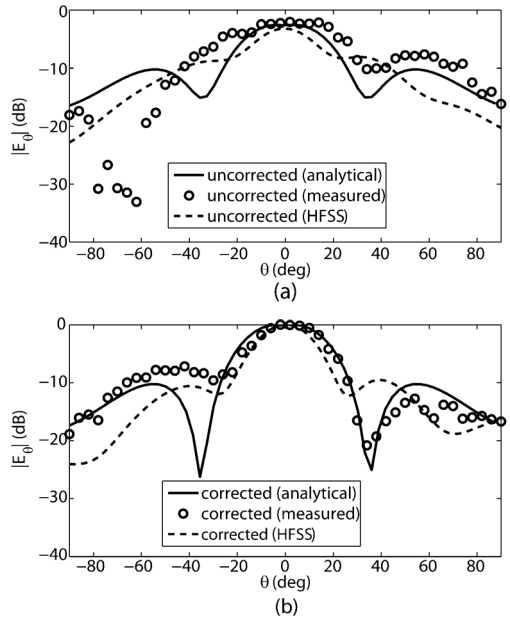

Fig. 8. Analytical, measured and simulated (a) uncorrected and (b) corrected patterns at 2.47 GHz in the y-z plane for the prototype on a spherical surface with a radius of $r = 20.32$ cm.

TABLE I
GAIN IMPROVEMENT VALUES FOR THE SELF-ADAPTING ARRAY

Radius	$G_{\Delta,meas.}$	$G_{\Delta,HFSS}$
20.32 cm	2.6 dBi	3.2 dBi
30.48 cm	1.7 dBi	1.9 dBi

Next, the antenna prototype was simulated in HFSS [36] on the nonconducting styrofoam spherical surface with $r = 20.32$ cm. Again, the phase compensation was computed using (5). The uncorrected and corrected radiation pattern from these computations are also shown in Fig. 8. Overall, good agreement between HFSS simulations and measurements can be observed. Furthermore, the gain improvement computed by HFSS is also shown in Table I and fair agreement with the measurements can be observed.

Then, the analytical computations computed by (7) for the antenna test platform were performed here for further validation. The results from these efforts are also shown in Fig. 8 with overall good agreement. It should also be mentioned that agreement between measurements, simulations and analytical computations was also observed in the x-z plane.

2) Spherical Surface With $r = 30.48$ cm: Next, the prototype 4 × 4 array with the embedded sensor circuit was attached to a nonconducting styrofoam spherical surface with a radius of $r = 30.48$ cm. The antenna and spherical surface was then again placed in the calibrated anechoic chamber and the patterns in the x-z and y-z planes were measured. The phase compensation values were computed using (5) and determined to be $\Delta\phi_{r1} = 89.2°$, $\Delta\phi_{r2} = 61.0°$, $\Delta\phi_{r3} = 38.8°$ and $\Delta\phi_{r4} = 10.0°$. The results from these measurements are shown in Figs. 9 and 10.

Again, the antenna prototype was simulated in HFSS on the styrofoam sphere with $r = 30.48$ cm and with the phase compensation computed using (5). The uncorrected and corrected radiation pattern from these computations are also shown in

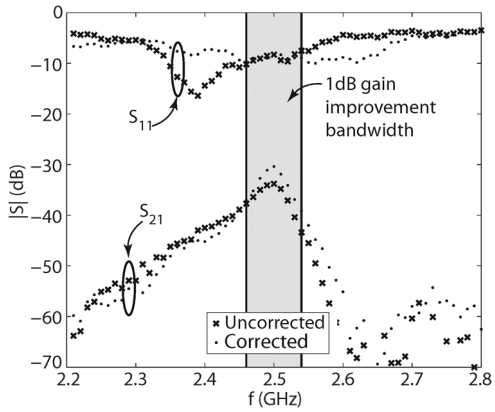

Fig. 9. Measured S-parameters for the prototype on a spherical surface with a radius of $r = 30.48$ cm.

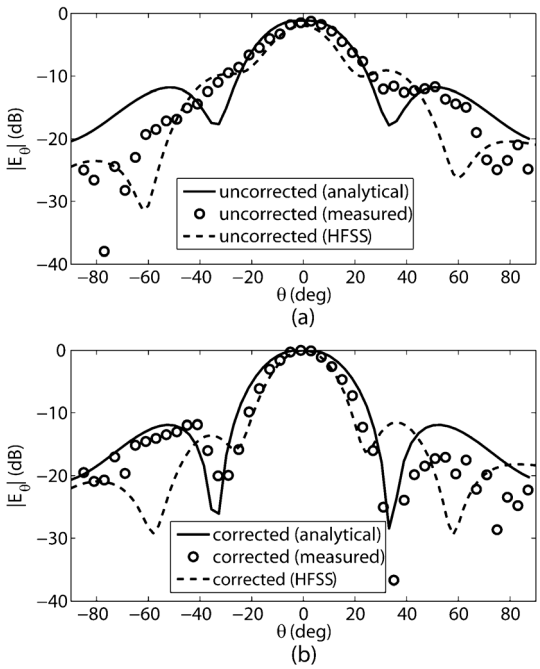

Fig. 10. Analytical, measured and simulated (a) uncorrected and (b) corrected patterns at 2.47 GHz in the y-z plane for the prototype on a spherical surface with a radius of $r = 30.32$ cm.

Fig. 10 and overall good agreement between HFSS simulations and measurements can be observed. The gain improvement computed by HFSS is also shown to agree in Table I with measurements.

The analytical computations were also compared to measurements in Fig. 10. Good agreement can be observed. As with the previous case for $r = 20.32$ cm, similar agreement between measurements, simulations and analytical computations was observed for the x-z plane.

The S-parameter results in Figs. 7 and 9 show that a 10 dB match can be achieved over the band where the maximum S_{21} values were measured. Furthermore, the S-parameters were measured with the receiving antenna along the z-axis of the sphere measuring E_θ. By comparing the S_{21} values for the uncorrected and corrected cases, a noticeable increase in gain can be observed. For a metric of measuring the gain improvement of the prototype array, a 1 dB gain improvement bandwidth (BW) was defined, denoted as $BW_{+1\,\mathrm{dB}}$. For $r = 20.32$ cm, $BW_{+1\,\mathrm{dB}} = 100$ MHz and for $r = 30.48$ cm, $BW_{+1\,\mathrm{dB}} = 80$ MHz. These values illustrate that a gain improvement of at least 1 dB is occurring over much of the BW of the array.

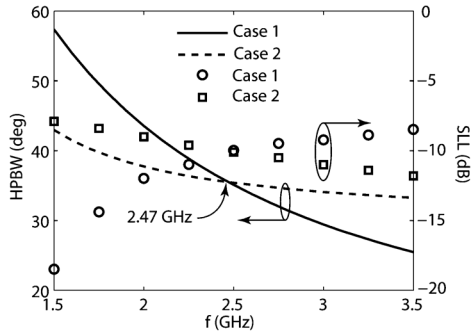

Fig. 11. Plot of the half-power beamwidth and side-lobe level for various inter-element spacing values.

C. Bandwidth Study

Finally, to further illustrate the bandwidth of the proposed phase-compensation method, the half-power beamwidth (HPBW) and Side-lobe levels (SLL) were computed for a 4 $\times$ 4 array on a spherical surface with $r = 20.32$ cm and an inter-element spacing of $S_x = 0.45\lambda$ and $S_y = 0.6\lambda$. More specifically, two cases were investigated. For case 1, the inter-element spacing was the same as the spacing for the results in Figs. 7–10. Then, using (6), the phase compensation was computed at 2.47 GHz (as with the spacing) and the source frequency was varied from 1.5 GHz to 3.5 GHz. HPBW and SLLs were then computed using (7) and these computations are shown in Fig. 11. It should be noted that for these computations, the spacing and phase compensation (computed at 2.47 GHz) were fixed in (7) and did not change with the source frequency. For case 2, the inter-element spacing and phase compensation changed with the source frequency and were not fixed. The HPBW and SLL computations using (7) are also shown in Fig. 11.

Case 1 was a study on how the radiation properties of the array change for an antenna with fixed phase compensation and spacing. This may be a design that is already manufactured and attached to a spherical surface and the spacing cannot be changed or the compensation if fixed. The results in Fig. 11 show that a trade-off between the HPBW and SLL exists as the frequency varies from the center frequency of 2.47 GHz. For frequencies below 2.47 GHz, the HPBW increases (i.e., becomes less directive) and the SLL decreases (i.e., the side-lobes decrease) and for frequencies above 2.47 GHz, the HPBW decreases (i.e., becomes more directive) and the SLL increases (i.e., the side-lobes increase).

Case 2 was studied to illustrate how the HPBW and SLL can be controlled by dynamically controlling the phase compensation and spacing of the array as the source frequency varies. The results show that the trade-off between HPBW and SLL is not as pronounced around the center frequency of 2.47 GHz.

V. Overall Discussion

The useful results of this research are summarized next:

1) The sensing circuit measurements in Fig. 3 show that a prototype sensor circuit can be used to measure the radius of curvature of a spherical surface and use this information

to apply the appropriate phase compensation. By using the analytical computations in (5), this compensation can be applied autonomously.

2) The pattern results in Fig. 5 show that the appropriate phase compensation can be analytically computed from the information on the shape of the sphere and antenna layout parameters (i.e., element spacing).
3) The S-parameter results in Figs. 7 and 9 demonstrate that good matching can be preserved over the 1 dB gain improvement BW for both radius of curvature values. Furthermore, it is shown that the gain is mostly improved near the designed operating frequency of 2.47 GHz.
4) The results in Table I and Figs. 8 and 10 show an overall agreement between measurements, simulations and analytical computations. However, some of the discrepancy between the results are believed to be due to the mutual coupling between elements. This coupling can be especially noticeable on conformal surfaces [37]. On the other hand, it has also been shown that it is possible to embed a simple sensor circuit into the design of a conformal antenna and use this circuit to efficiently measure the surface of the array and autonomously apply the appropriate phase compensation for radiation pattern recovery.
5) Finally, the amount of allowable beamwidth and side-lobes vary by application and the results in Fig. 11 can be used to help define the bandwidth of the phase compensation method.

VI. Conclusion

Simple analytical phase compensation expressions in terms of the antenna array design parameters and spherical surface geometries have been derived here for the purpose of developing an autonomous self-adapting phased-array conformal antenna prototype. Initially, the phase compensation expressions were validated experimentally at 2.47 GHz with a precisely controlled 4×4 phased-array antenna test platform with individual microstrip antenna elements and voltage controlled phase shifters. After this agreement between the analytical expressions and the measurements was demonstrated, a 4×4 antenna prototype with an embedded sensor and phase-compensation circuitry was developed at 2.47 GHz. The sensor circuit was designed with the new expressions presented in this paper and used to measure the spherical surface geometries and apply the appropriate phase compensation values for $r = 20.32$ cm and 30.48 cm. Overall, it was shown with measurements, simulations and analytical computations that the correct sensor circuit could be designed and used to autonomously recover the radiation pattern of the 4×4 microstrip array on two different spherical surfaces.

References

[1] H. Schippers, G. Spalluto, and G. Vos, "Radiation analysis of conformal phased array antennas on distorted structures," in *Proc. 12th Int. Conf. Antennas and Propagation*, Mar. 31–Apr. 3 2003, pp. 160–163.

[2] H. Schippers, J. Verpoorte, P. Jorna, A. Hulzinga, A. Meijerink, C. Roeloffzen, R. G. Heideman, A. Leinse, and M. Wintels, "Conformal phased array with beam forming on airborne satellite communication," in *Proc. Int. ITG Workshop on Smart Antennas*, Feb. 26–27, 2008, pp. 343–350.

[3] H. Schippers, P. Knott, T. Deloues, P. Lacomme, and M. R. Scherbarth, "Vibrating antennas and compensation techniques research in NATO/RTO/SET 087/RTG 50," in *Proc. IEEE Aerospace Conf.*, Mar. 3–10, 2007, pp. 1–13.

[4] P. Jorna, H. Schippers, and J. Verpoorte, "Beam synthesis for conformal array antennas with efficient tapering," presented at the 5th Eur. Workshop on Conformal Antennas, Bristol, U.K., Sep. 11–12, 2007.

[5] P. Knott, "Deformation and vibration of conformal antenna arrays and compensation techniques," in *Proc. Meet. RTO-MP-AVT-141*, 2006, pp. 1–12, paper 19.

[6] R. C. Hansen, *Phased Array Antennas*. Hoboken, NJ, USA: Wiley, 1998.

[7] R. L. Haupt, *Antenna Arrays: A Computational Approach*. Hoboken, NJ, USA: Wiley, 2010, pp. 287–315.

[8] L. Josefsson and P. Persson, *Conformal Array Antenna Theory and Design*. Hoboken, NJ, USA: Wiley, 2006.

[9] M. Klemm and G. Troester, "Textile UWB antennas for wireless body area networks," *IEEE Trans. Antennas Propag.*, vol. 54, no. 11, pp. 3192–3197, Nov. 2006.

[10] T. F. Kennedy, P. W. Fink, A. W. Chu, N. J. Champagne, G. Y. Lin, and M. A. Khayat, "Body-worn E-textile antennas: The good, the low-mass, the conformal," *IEEE Trans. Antennas Propag.*, vol. 57, no. 4, pp. 910–918, Apr. 2009.

[11] P. Salonen, Y. Rahmat-Samii, M. Schaffrath, and M. Kivikoski, "Effect of textile materials on wearable antenna performance: A case study of GPS antennas," in *Proc. IEEE Int. Symp. Antennas Propag. Soc.*, 2004, vol. 1, pp. 459–462.

[12] D. Psychoudakis, G. Y. Lee, C.-C. Chen, and J. L. Volakis, "Estimating diversity for body-worn antennas," presented at the 3rd Eur. Conf. Antennas and Propagation (EuCAP), Berlin, Germany, Mar. 23–27, 2009.

[13] P. J. Callus, "Conformal load-bearing antenna structure for australian defense force aircraft," in *DSTO Platforms Sciences Laboratory*, Victoria, Australia, 2007.

[14] Y. Byram, Y. Zhou, B. S. Shim, S. Xu, J. Zhu, N. A. Kotov, and J. L. Volakis, "E-textile conductors and polymer composites for conformal lightweight antennas," *IEEE Trans. Antennas Propag.*, vol. 56, no. 8, pp. 2732–2736, Aug. 2010.

[15] S. E. Morris, Y. Bayram, L. Zhang, Z. Wang, M. Shtein, and J. L. Volakis, "High-strength, metalized fibers for conformal load bearing antenna applicaitions," *IEEE Trans. Antennas Propag.*, vol. 59, no. 9, pp. 3458–3462, Sep. 2011.

[16] Z. Wang, L. Zhang, Y. Bayram, and J. L. Volakis, "Multilayer printing of embroidered RF circuits on polymer composites," presented at the IEEE Int. Symp. Dig. Antennas Propag. Soc., Spokane, WA, Jul. 3–8, 2011.

[17] B. D. Braaten, M. A. Aziz, S. Roy, S. Nariyal, I. Irfanullah, N. F. Chamberlain, M. T. Reich, and D. E. Anagnostou, "A Self-Adapting Flexible (SELFLEX) antenna array for changing conformal surface applications," *IEEE Trans. Antennas Propag.*, vol. 61, no. 2, pp. 655–665, Feb. 2013.

[18] B. D. Braaten, I. Ullah, S. Nariyal, A. Naqvi, M. Iskander, and D. E. Anagnostou, "Scanning characteristics of a self-adapting phased-array antenna on a wedge-shaped conformal surface," in *Proc. IEEE Int. Symp. Dig. Antennas Propag. Soc.*, Orlando, FL, Jul. 7–13, 2013, pp. 1056–1057.

[19] K. Wincza and S. Gruszczynski, "Influence of curvature radius on radiation patterns in multibeam conformal antennas," in *Proc. 36th Eur. Microw. Conf.*, Sep. 10–15, 2006, pp. 1410–1413.

[20] E. Kiely, G. Washington, and J. Bernhard, "Design and development of smart microstrip patch antennas," *Smart Mater. Struct.*, vol. 7, no. 6, pp. 792–800.

[21] J. Huang, "Bandwidth study of microstrip reflectarray and a novel phased reflectarray concept," in *Proc. IEEE Int. Symp. Antennas Propag.*, Newport Beach, CA, Jun. 18–23, 1995, pp. 582–585.

[22] N. Tiercelin, P. Coquet, R. Sauleau, V. Senez, and H. Fujita, "Polydimethylsiloxane membranes for millimeter-wave planar ultra flexible antennas," *J. Micromech. Microeng.*, vol. 16, no. 11, pp. 2389–2395.

[23] P. L. O'Donovan and A. W. Rudge, "Adaptive control of a flexible linear array," *Electron. Lett.*, vol. 9, no. 6, pp. 121–122, Mar. 22, 1973.

[24] J.-L. Guo and J.-Y. Li, "Pattern synthesis of conformal array antenna in the presence of platform using differential evolution algorithm," *IEEE Trans. Antennas Propag.*, vol. 57, no. 9, pp. 2615–2621, Sep. 2009.

[25] E. Lier, D. Purdy, and G. Kautz, "Calibration and Integrated Beam Control/Conditioning System for Phased-Array Antennas," U.S. Patent 6163296, Dec. 19, 2000.

[26] E. Lier, D. Purdy, J. Ashe, and G. Kautz, "An on-board integrated beam conditioning system for active phased array satellite antennas," in *Proc. IEEE Int. Conf. Phased Array Systems and Technology*, Dana Point, CA, May 21–25, 2000, pp. 509–512.

[27] D. Purdy, J. Ashe, and E. Lier, "System and Method for Efficiently Characterizing the Elements in an Array Antenna," U.S. Patent 2002/0171583 A1, Nov. 21, 2002.
[28] E. Lier, M. Zemlyansky, D. Purdy, and D. Farina, "Phased array calibration and characterization based on orthogonal coding: Theory and experimental validation," in *Proc. IEEE Int. Symp. Phased Array Systems and Technology (ARRAY)*, Oct. 12–15, 2010, pp. 271–278.
[29] Y. Wu, K. F. Warnick, and C. Jin, "Design study of an L-band phaed array feed for wide-field surveys and vibration compensation on FAST," *IEEE Trans. Antennas Propag.*, vol. 61, no. 6, pp. 3026–3033, Jun. 2013.
[30] I. Chiba, K. Hariu, S. Sato, and S. Mano, "A projection method providing low sidelobe pattern in conformal array antennas," in *Proc. IEEE Int. Symp. Dig. Antennas Propag. Soc.*, Jun. 26–30, 1989.
[31] T. J. Seidel, W. S. T. Rowe, and K. Ghorbani, "Passive compensation of beam shift in a bending array," *Progr. Electrom. Res.*, vol. 29, pp. 41–53, 2012.
[32] Hittite Microwave Corporation [Online]. Available: http://www.hittite.com
[33] Spectra Symbol [Online]. Available: http://www.spectrasymbol.com
[34] Rogers Corporation [Online]. Available: http://www.rogerscorp.com
[35] I. J. Bahl and P. Bhartia, *Microstrip Antennas*. Dedham, MA, USA: Artech House, Inc., 1980, p. 50.
[36] Ansys, Inc., Ansoft HFSS, Version 13.0.1 [Online]. Available: http://www.ansoft.com
[37] I. Ullah, S. Nariyal, S. Roy, M. M. Masud, B. Ijaz, A. Aftikhar, S. A. Naqvi, and B. D. Braaten, "A note on the fundamental maximum gain limit of the projection method for conformal phased array antennas," in *IEEE Int. Conf. Wireless Inf. Tech. Syst.*, Maui, HI, USA, Nov. 11–16, 2012.

Benjamin D. Braaten (S'02–M'09) received the Ph.D. degree in electrical engineering from North Dakota State University, Fargo, ND, USA, in 2009.

During the 2009 Fall semester, he held a post doctoral research position at the South Dakota School of Mines and Technology, Rapid City, SD, USA. Currently, he is an Assistant Professor in the Electrical and Computer Engineering Department, North Dakota State University, Fargo, ND, USA. His research interests include printed antennas, conformal self-adapting antennas, microwave devices, topics in EMC, and methods in computational electromagnetics.

Sayan Roy (S'10) was born in Chandannagar, India, in 1988. He received the B.Tech. degree in electronics and communication engineering from the West Bengal University of Technology, Kolkata, India, in 2010 and the M.S. degree in electrical and computer engineering from North Dakota State University, Fargo, ND, USA, in 2012. Currently, he is pursuing the Ph.D. degree in electrical and computer engineering at North Dakota State University, Fargo, ND, USA.

His research interests include microwave antennas, printed antenna array, conformal self-adapting antennas, RFID, topics in EMC, and wearable antennas.

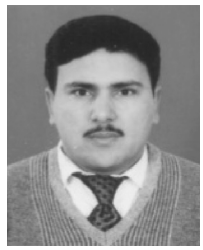

Irfan Irfanullah (S'05–M'07) received the M.S. degree in electrical engineering from the University of Engineering and Technology, Lahore, Pakistan, in 2007. He is currently pursuing the Ph.D. degree in conformal smart antennas at North Dakota State University, Fargo, ND, USA.

He is a faculty member of the COMSATS Institute of Information Technology, Pakistan, and His research interests include the antenna arrays, signal integrity, and topics in EMC.

Sanjay Nariyal (S'10–M'13) received the B.S. and M.S. degrees in Electrical Engineering from North Dakota State University, Fargo, ND, USA, in 2010 and 2013, respectively.

He was a Graduate Research/Teaching Assistant in the Electrical and Computer Engineering Department at North Dakota State University, Fargo, ND, USA, and with the Center for Nanoscale Science and Engineering, Fargo, ND, USA. Currently, he is an Engineer Quality I at John Deere Electronic Solutions, Fargo, ND, USA. His research interests include antennas and issues in electromagnetic compatibility.

Dimitris E. Anagnostou (S'98–M'05–SM'10) received the B.S.E.E. degree from the Democritus University of Thrace, Greece, in 2000, and the M.S.E.E. and Ph.D. degrees from the University of New Mexico, Albuquerque, NM, USA, in 2002 and 2005, respectively.

From 2005 to 2006, he was a Postdoctoral Fellow at the Georgia Institute of Technology, Atlanta, GA, USA. In 2007, he joined the faculty of the Electrical and Computer Engineering Department, South Dakota School of Mines and Technology, Rapid City, SD, USA, where he is currently Associate Professor. In 2011, he was an AFRL Summer Faculty Fellow with the Kirtland Air Force Base, NM, USA. He has authored or coauthored more than 80 papers published in refereed journals and symposia proceedings and he holds one U.S. patent on MEMS reconfigurable antennas. His interests include reconfigurable, autonomous, flexible, electrically-small and miniaturized antennas and arrays; phase-change materials; analytical design methods and equivalent circuits of antennas and microwave components; metamaterial applications; direct-write; security printing; "green" RF electronics on paper and organic substrates; applications of artificial dielectrics and superstrates; leaky-wave antennas; cavity resonance antennas; antennas integrated with photovoltaic cells; RF-MEMS; propagation in tunnels; and microwave packaging.

Dr. Anagnostou is a recipient of the DARPA Young Faculty Award by the U.S. Department of Defense and the IEEE John Kraus Antenna Award by the IEEE Antennas and Propagation Society (AP-S). He has also been recognized as a distinguished scientist living abroad by the Hellenic Ministry of Defense. He serves as an Associate Editor for the IEEE TRANSACTIONS ON ANTENNAS AND PROPAGATION, a member of the IEEE APS Educational Committee, a member of the TPC and session chair for the IEEE AP-S International Symposia, and a reviewer for more than 15 international journal publications including the IEEE TRANSACTIONS ON ANTENNAS AND PROPAGATION, the IEEE TRANSACTIONS ON MICROWAVE THEORY AND TECHNOLOGY, the *IEEE Antennas and Propagation Magazine*, *AWPL*, *MWCL*. He has given two workshop presentations at IEEE AP-S and IEEE MTT-S International Symposia. He is a member of Eta Kappa Nu, ASEE, and of the Technical Chamber of Greece.